ISSN: 2148-9173 **Vol: 9 Issue:4 December 2022**

International Journal of Environment and Geoinformatics (IJEGEO) is an international, multidisciplinary, peer reviewed, open access journal.

The Detection of the Buried Pipes Using GPR in Utility Works: A Case Study

Yalçın YILMAZ , Arzu SOYCAN

Abstracting and Indexing: TR DIZIN, DOAJ, Index Copernicus, OAJI, Scientific Indexing Services, International Scientific Indexing, Journal Factor, Google Scholar, Ulrich's Periodicals Directory, WorldCat, DRJI, ResearchBib, SOBIAD

International Journal of Environment and Geoinformatics 9(4):124-137 (2022)

Research Article

The Detection of the Buried Pipes Using GPR in Utility Works: A Case Study

Yalçın Yilmaz*, Arzu Soycan

Yildiz Technical University, Faculty of Civil Engineering,, Department of Geomatic Engineering, Istanbul, TURKIYE

* Corresponding author: Y. Yımaz
E-mail: yilmazy@yildiz.edu.tr

Received: 22.03.2022
Accepted 18.06.2022

How to cite: Yilmaz and Soycan (2022). The Detection of the Buried Pipes Using GPR in Utility Works: A Case Study, *International Journal of Environment and Geoinformatics (IJEGEO)*, 9(4):124- 000. doi. 10.30897/ijegeo.1091852

Abstract

The increasing population and accordingly the new settlement ultimately need for the utility. Location and attribute information of utilities significantly affect the maintenance, repair and construction of utilities. The lack of such information causes accidents resulting in material and moral damages in utility excavations 'especially in the city'. The lack of information on utility works in our country raises problems such as damage to another utility during the work, being unable to complete the work on time, affecting vehicle and pedestrian traffic. This study has focused on the detectability of utilities with unknown location and attribute (diameter) using a ground penetrating radar (GPR) based on simulation model and field surveys. An antenna frequency of 300 MHz was chosen in both applications. The analysis of the data obtained from the simulation model revealed positive results in terms of the usability of the GPR for the determination of location and attributes in utility works. Furthermore, the results of the field studies demonstrated that if the dielectric constants of a utility element and of its location are close, data on the utility cannot be obtained; if the trench base is narrow, it gives a hyperbola reflection like pipeline; and if it is not analyzed carefully, this pseudo- reflection may lead to mistakes. The field study shows that if there are no continuous hyperbola reflections on consecutive radargrams, the possibility that the reflection may not be due to pipeline should be considered.

Keywords: Utility, GPR, Utility Positioning, Utility Detection

Introduction

Equipment to provide electricity, water, natural gas, treatment, any transportation and communication services, all which are common needs of people, are called utility. As a result of the rapid growth of the population and the spread of new technologies, utilities also continue to expand. Therefore, old utilities are replaced with new ones or the existing utilities are updated due to dislocation or faults, which plays an important role in utility sector (Anspach, 1996). Existing utilities and associated structures are vital in utility works. These structures may be a reference for new works, while they may also pose risks for them (Costello et al., 2007). The majority of these risks are caused by the fact that the location and attribute information of existing lines are incomplete, wrong or out-of-date. Works carried out based on incomplete or wrong information have material and moral consequences. When the accidents related to the utility works are examined in Turkey, approximately 8400 natural gas line damages are seen and their cost is about $1.65 million [URL1]. If other utilities are taken into account, the cost will increase even more. The accurate positioning of utilities and determining the existing lines during construction are essential to minimize such situations. From this point of view, we can investigate the positioning methods used in utility works under the two main headings as shown in Figure 1.

This study aimed to detect buried utilities that have no location and attribute information. In this regard, the GPR method, a closed trench positioning method, was preferred since it is a non-destructive, rapid (Jeng and Chen, 2012) and material-independent system. The other reason of the preference is that other closed trench positioning methods are used specifically according to the type of utility. (E.g. EML for metal pipelines.)

GPR has been used in many fields (archaeological studies, glacier studies, etc.) from past to present. One of them is the determination of buried utilities. When the literature is reviewed, the following studies about usability of GPR on detecting pipelines stand out.

Chow and Rees (1989) investigated the usability of GPR in determination of agricultural water drainage channels and pipelines buried under different types of soil. The study results emphasized that the dielectric constant of the object as well as the size and depth of the object are important in determinations with GPR.

Kurt et al. (2009) investigated the determinability of location, size and physical characteristics of buried pipelines. For this, they performed both laboratory and field applications. In the study, it was stated that it is possible to make comment on the physical characteristic of pipe by analyzing the hyperbolas of the waves reflected from objects and investigating the amplitude differences of location and size.

In a study by Metwaly (2015) in an asphalt road in Mecca, he investigated the usability of GPR in utility works. In his study, it was stated that the physical characteristics of a utility (such as potable water pipeline, sewer line) can be understood based on the sizes of hyperbolas reflected from objects. It was also emphasized that information on the region can be obtained with GPR before an excavation work.

The other paper about GPR was carried out by Ristic et al. (2009). They studied about estimating the radius of a cylindrical object and the wave propagation velocity from GPR data. Prego et al. (2017) did research about efficient GPR data acquisiton to detect underground pipes using various types and configurations of piping with different frekans GPR antennas.

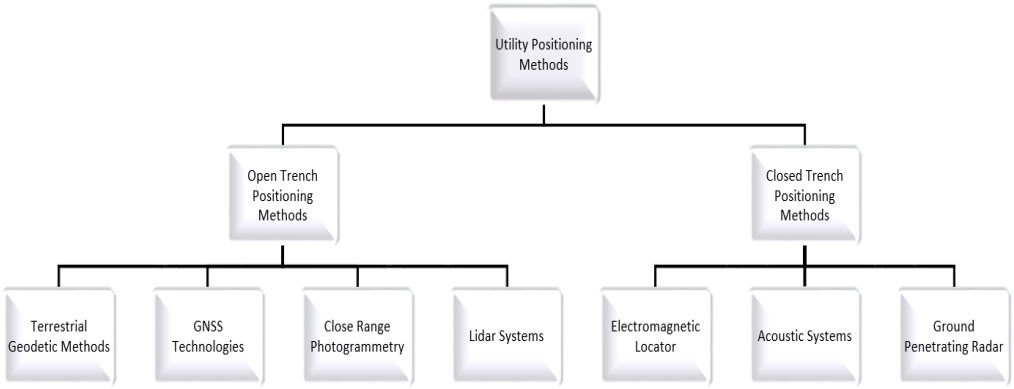

Fig. 1. Utility Positioning Methods.

Šarlah et al. (2020) studied about utility mapping with Ground Penetrating Radar-Terrestial Positioning System integration. The 400 MHz antenna was used in study and carried out in two urban site. When the results were examined, it seemed that the vertical accuray was 4-11 cm and horizontal accuracy was 6-15 cm. They stated that GPR-TPS was useful for horizontal and vertical accuracy requirements in Slovenia.

In our study, 2 different data sets, including simulation profile model data and actual field data, were used to determine the usability of GPR in identifying utilities.

The profile model was designed with a width of 20 meters and a length of 10 meters. In the simulation model, the storm water and waste water lines were sloped by -2% along the length of the profile. A total of 55 profiles were scanned at an interval of 0.20 meter between them. The actual field data were obtained from 11 profile scans performed on a route of 14 m within the Yildiz Technical University (YTU) Davutpaşa Campus (Figure 2). Unlike other studies, although the simulation model yielded results for utilities, the actual field data had no clear reflection for the utility element. In the study, the reasons of this situation were also investigated.

Fig. 2. Study area.

Materials and Methods

GPR is an easily applied technology, which shows shallow subsurface in detail using high-frequency electromagnetic waves, has a high-speed data acquisition and often used in geophysical studies. GPR assembly was first applied by Stern in 1930 to estimate the underwater depth of glaciers in Austria (Blindow et al., 2007). It took its current form in the 1970s and was commercially introduced to the market.

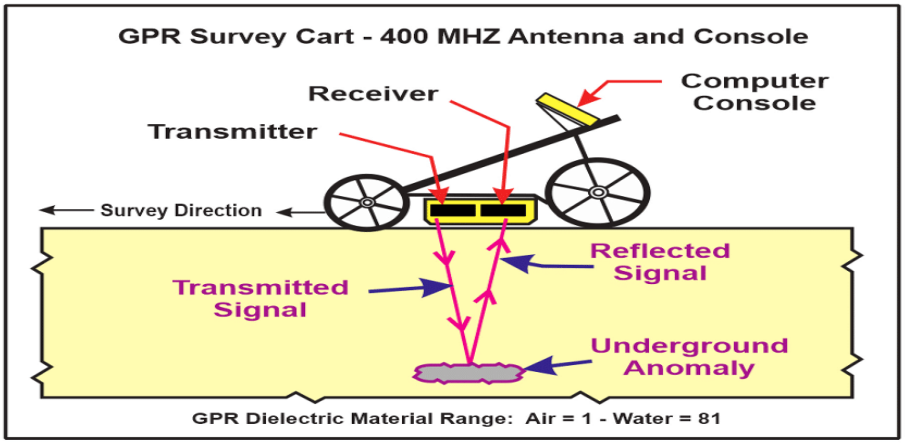

Fig.3. Ground penetrating radar components (GPR, 2017).

A GPR consists of a receiver antenna, a transmitter antenna and a control unit (Figure 3). The transmitter antenna generates an electromagnetic signal radiating into the soil. The generated signal radiates underground conically. When the electromagnetic signal to underground encounters with objects or surfaces with different dielectric characteristics, a portion of it reflects back, while a portion of it continues to move deeper. The reflected signals are collected by the receiver antenna. Such signals recorded by reflection are called "radargram" (Figure 4).

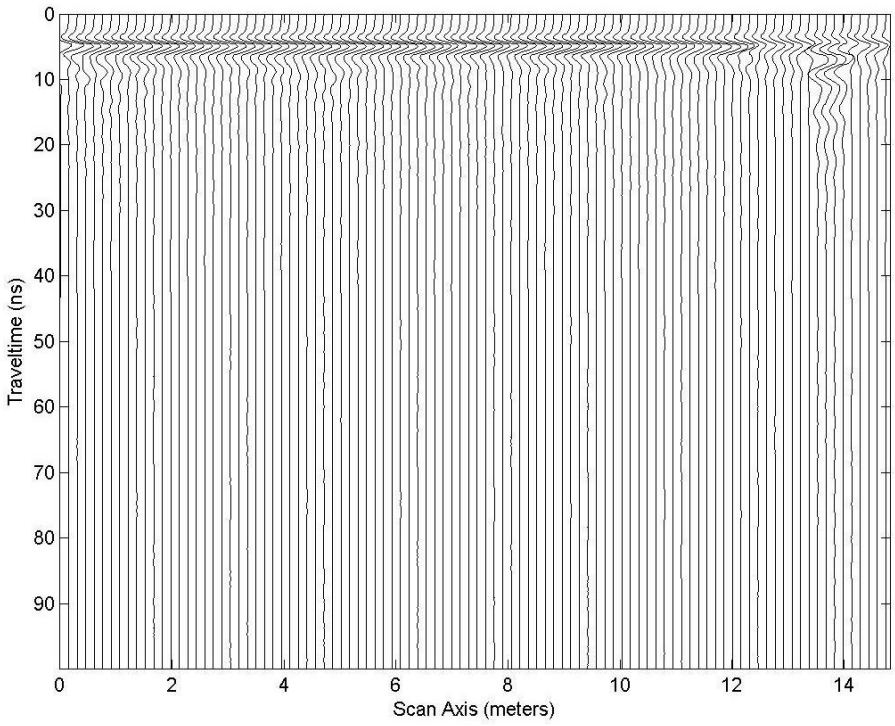

Fig. 4. Radargram.

Measurement method using GPR is based on the electromagnetic theory. Therefore, factors affecting electromagnetic wave radiation also affect the measurement results. These factors include ambient dielectric permittivity, electrical conductivity and magnetic permeability. Dielectric permittivity is the most important factor that affect signal radiation intensity, vertical and horizontal resolution and reflection constants. For the dielectric permittivity values of the materials in the simulation model established (Figure 6) in the application, the values in Tables (Öztürk, 2011; Leckebusch, 2003) were taken into account. The information on the simulation profile (dielectric constant (Ɛr), magnetic permeability (μr), electrical resistivity (ρr), distance to profile, depth pipe diameter, material) are shown in Table 1. The used abbreviations in Table 1 are P.W (Potable Water Pipeline), W.W (Waste Water Pipeline), and S.W (Storm Water Pipeline).

Table 1. Attributes of the materials

Object	Material	Depth (m)	Diameter (m)	ε_r	μ_r	ρ_r (Ω.m)	Distance to baseline (m)
P.W1	Polyethylene	1	0.18	2.5	1	10^{12}	5.2
P.W2	Polyethylene	1	0.16	2.5	1	10^{12}	14.6
W.W	Concrete	3.20	0.50	10	1	10^{2}	9
S.W	Concrete	2	0.30	8	1	10^{2}	11
Asphalt	-	0.20	-	3	1	10^{2}	-
Trench	Dry Sand	5	-	5	1	10^{5}	-
Ground	Sandy Soil	6	-	2.6	1	700	-

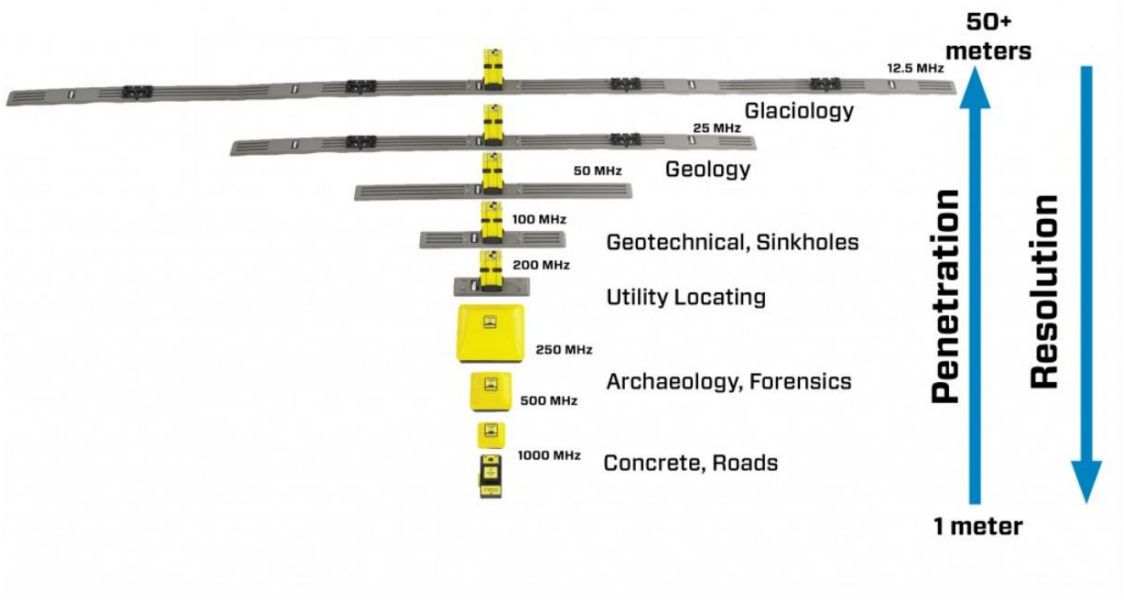

Fig. 5. The antennas according to applications [URL2].

In this application, considering the pipe depth and pipe diameter, the antenna center frequency is taken as 300 MHz for both field study and simulation, taking into account the values given in Figure 5.

The simulation data was obtained from the profile scans made with MatGPR 3.1 software (Tzanis, 2010). At the signal penetration length of 138.39 ns, the number of sampling per track was 376, and the total number of tracks was 380. The field data were obtained with Geoscanner GCB antenna with a center frequency of 300 MHz. At the signal penetration length of 100 ns, the number of sampling per track was 800, and the total number of tracks was 429.

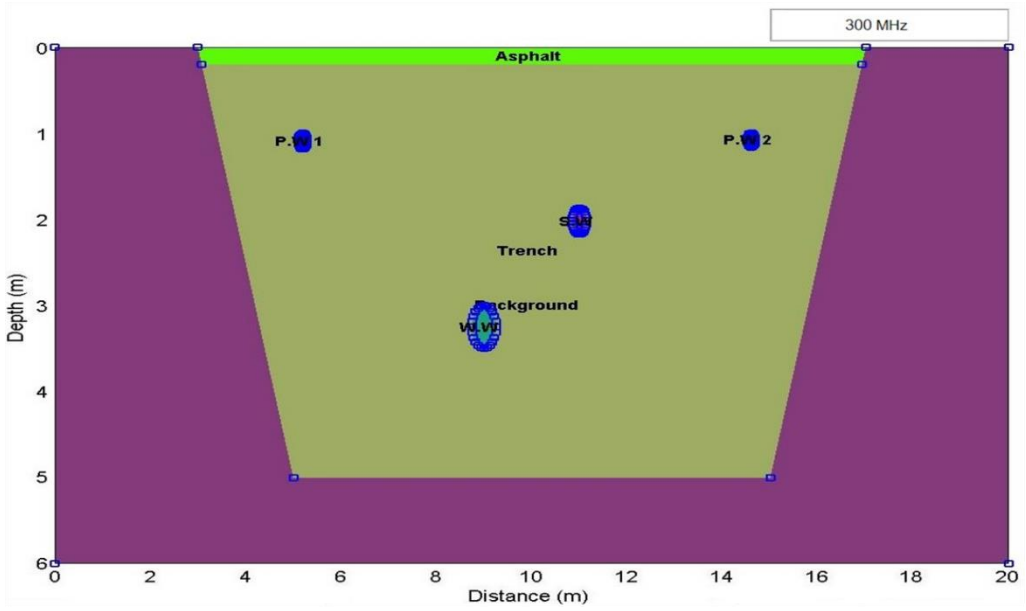

Fig. 6. Profile of the Simulation Model

Processing of GPR Data and 3D Modelling

There are two ways to convert the GPR data to the application. The first one is to reveal the anomaly or target location in the received data as a section, a plan or a volume, which are the same for all geophysical (seismic, etc.) methods. The second one is to identify measurable wave characteristics such as speed, attenuation, and impedance and to convert these characteristics to application-specific quantities. Because it is not possible to fully describe the physical status of the researched environment from raw data. Therefore, raw data should be subjected to certain data processing steps. These data processing steps include the use of customized filters to eliminate noise from the raw data as well as to regulate and enhance digital reflections (Jol, 2008; Goodman and Piro, 2013).

The data processing steps can be investigated under two headings (basic and advanced data processing) according to the purpose of the application.

The basic data processing steps are adjusting the signal position, removing any low-frequency data (dewow), amplitude gain and background removal.

The adjustment of the signal position is the subtraction of the time elapsed from which electromagnetic wave emits from the transmitter and contacts with the surface from the first time, from the data. This is necessary for accurate calculation of the position of anomaly to be identified.

The Dewow effect occurs because the receiver is close to the transmitter. The field near the transmitter contains low-frequency energies associated with electrostatic and inductive fields decreasing rapidly with distance. These low-frequency energies provide a component with a slow time-dependent change in field measurements. This causes the received signals to exceed or fall below the base level. These components may prevent the perception of the real situation. This effect is called “wow” in the literature of GPR. Elimination of this effect is called “dewow” (Jol, 2008).

Amplitude gain is the process of strengthening the appearance of reflected waves due to situations such as signal attenuation. Most data collected with a GPR require a gain process after the measurement to visualize the reflected radar waves. It is based on raising the values by multiplying successive portions of a track with a constant.

Background removal process is the process of removing horizontal constant repetitive data in the image, which is called as the ringing effect.
Advanced data processing steps are Filtering, Deconvolution, and Migration.

Filtering includes low-pass, high-pass and band-pass filtering processes. These provide visibility into the data at any frequency range or any wavelength (long or short). Deconvolution is a signal processing method to help reduce multiple reflections and echoes recorded on the radargram as well as to minimize the effects of the transmitted wave from the source. Migration process is a signal processing to collapse hyperbola reflections including point-source reflections by collecting the whole energy from hyperbolas along the radargram and placing it at the top of hyperbolas. It collapses hyperbolas as well as allows for reorienting the reflecting surfaces and correctly positioning them as seen Figure 13. The migration process is based on electromagnetic wave velocity. In this study velocity was determined using hyperbola reflection because there is no accurate information about the layer thickness in real site. Moreover, MatGPR 3.1 Software used data process have an option to get velocity from hyperbola reflection.

The data process steps and modeling steps applied for both data sets in this study are given in Figure 7. MatGPR 3.1 software was used in the application of these process steps, while Voxler 4.0 (Golden Software, 2015) software was used in the 3D Modeling.

Results and Discussion
Simulation Model

Firstly, a local coordinating process was performed on 51 radargrams obtained from the scan on the simulation model (Figure8). Figure 8 indicates the scan track number, the distance of trace from the profile origin (x), the distance between profiles (y) and the depth (z), respectively (i.e. travel times axis on radargram). After this process, each scan track has x, y, z local coordinate values.
After then, the process steps in Figure 7 were applied on each radargram. Adjusting signal position, dewow, bandpass filtering, gain and background removal processes were applied respectively on a radargram obtained from the model. Figure 9 shows the sample data and the process steps applied on the data.

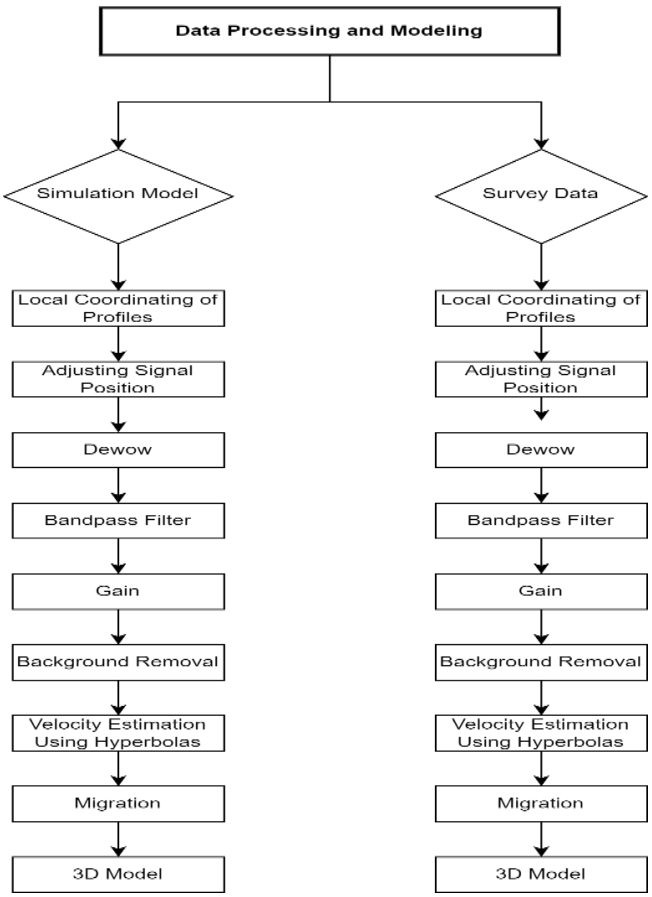

Fig. 7. Data Process Steps and 3-D Modeling.

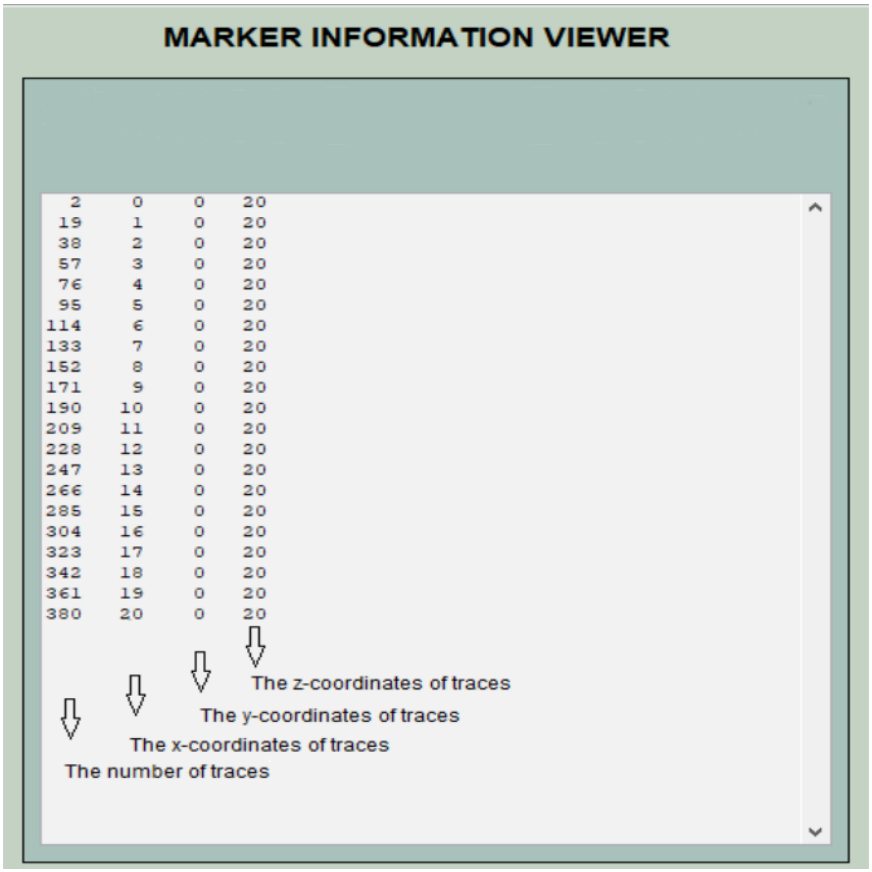

Fig. 8. The marker information of the traces.

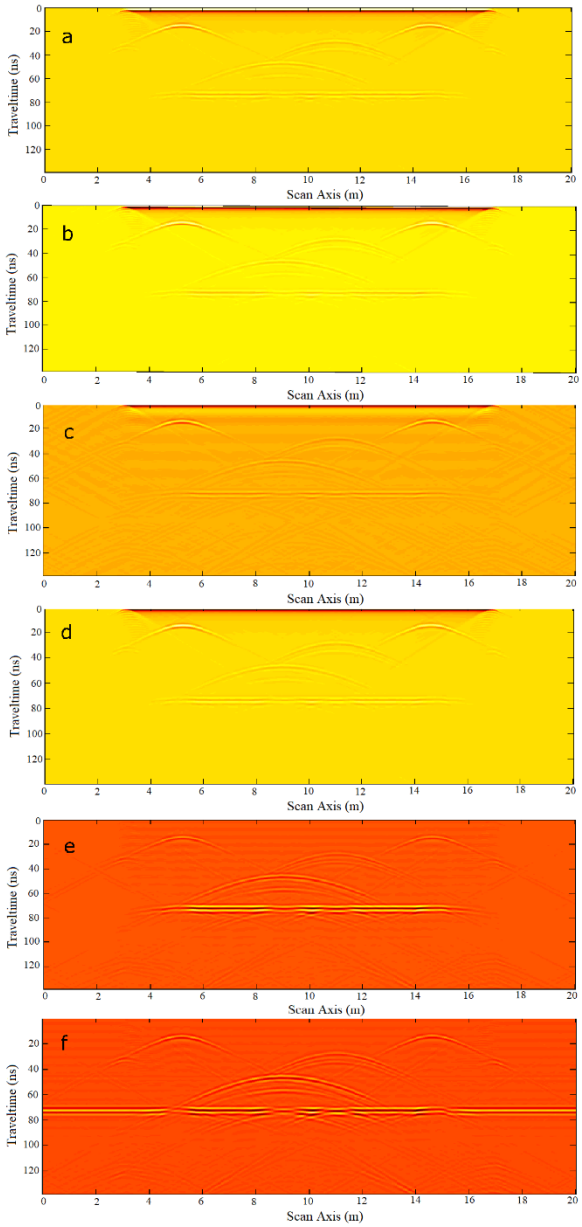

Fig. 9. a. Raw data b. Signal Adjusting c. Dewow d. Bandpass Filtering e. Gain f. Background Removal.

The depth (Z) was obtained from the hyperbolas reflected from anomaly using Equation (1), and the average medium velocity (V_m) was obtained from depth and t0 using Equation (2) (Daniels, 1989).

$$Z = \frac{|x|}{2\sqrt{(\frac{t}{t_0})^2 - 1}} (1)$$

$$V_m = Z/(\frac{t_0}{2}) (2)$$

x= distance between the vertex of hyperbola and another point taken on a hyperbola
t0=two- way travel time of the vertex of the hyperbola
t= two-way travel time of other point taken on the hyperbola.

Where k represents the number of points, e is the position of a point in the east-west direction, and n stands for the position of a point in the north-southern direction (Table 1).

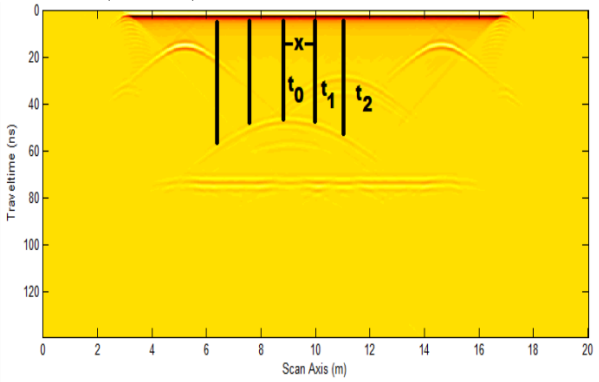

Fig. 10. Determination of depth from hyperbola reflection.

Figure 10 illustrates representation of the equation parameters on the radargram. The average velocity was 0.16 m/ns, and the depth was 1.01 meter, which were calculated from the first hyperbola on the 3rd radargram gained from the profile scans performed on the simulation model.

The pipe radius and locations were obtained from the reflections on each radargram using Z and V_m values in MatGPR 3.1 software. An example is given in Figure 11.

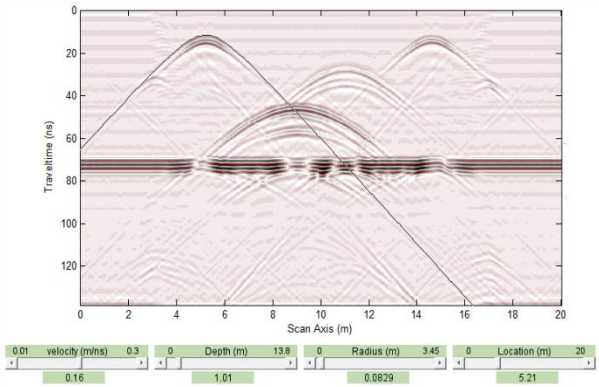

Fig. 11. Determination of velocity, depth, radius and location from hyperbola reflection on radargram.

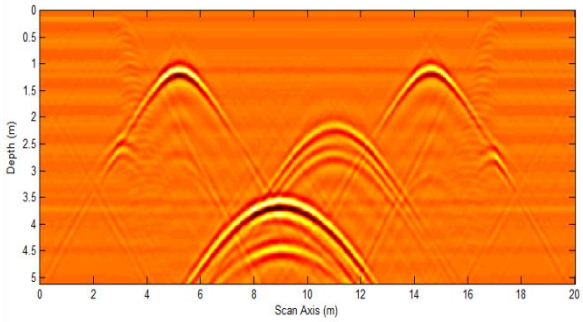

Fig. 12. Radargram obtained from the Time-Depth Conversion.

It was limited with a portion of 65 ns containing hyperbola anomaly from each radargram that are necessary for the study. Time-depth conversion was

performed using velocity, and the radargram in Figure 12 was obtained.

Migration process was carried out on the same radargram, and energy was concentrated at the peak point of the hyperbola, and the reflections were made into a point object (Figure 13). This was performed to all the radargrams and the current radargrams were acquired after the migration.

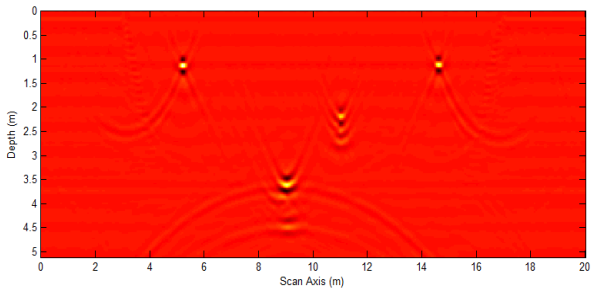

Fig.13. Migration

From 51 radargrams, 11 radargrams were selected at 1 m intervals. Table S1 (in supplementary) shows the comparison of the location, depth, and diameter information of each anomaly determined on these radargrams with the actual values. When the results of P.W1 and P.W2 were analyzed, the location difference was found 1 cm, the depth difference was found 1 cm, and the diameter differences were found 1.42 cm for P.W1 and 1.5 cm for P.W2. When the results of W.W and S.W were investigated, the location difference was found 1 cm, the depth differences were found 15 - 18 cm for W.W and 1 - 5 cm for S.W, and the diameter differences were found 12.8 cm for W.W and 6.6 cm for S.W. Also, the slope of -2% given for both lines were calculated as -2.1% and -2.2% from the data in Table S1, respectively. When the results are investigated, it is seen that the error amount in the location and attribute data of the utilities increases with increasing depth. It was observed that the acquisite diameters were proportional to each other as in the actual data.

The data were gridded with MatGPR 3.1 software to make the radargrams 3-dimensional after completing local coordinating and migration processes. During this process, the software uses index values assigned according to x, y, z and amplitude value of each track. In gridding, the sampling interval in x and y direction was taken as 0.20 m, and the data were gridded based on the absolute track value, which is the software's default method. The 3D isosurface obtained from the simulation with MatGPR 3.1 software is shown in Figure 14.

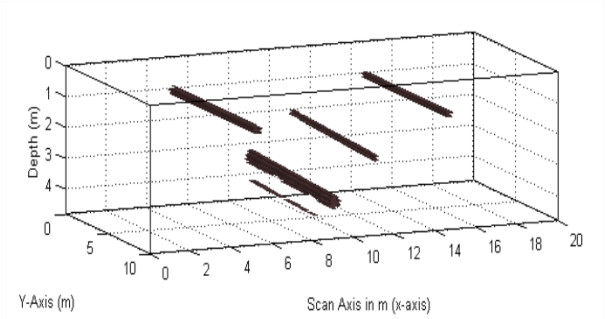

Fig. 14. Isosurface generated with MatGPR 3.1

The radargram data were saved in the ASCII format. These data were gridded with the inverse weighted distance method using Voxler 4.0 software to generate 3D isosurface (Figure 15). In the figure, the depth is shown as absolute value and represents below the ground.

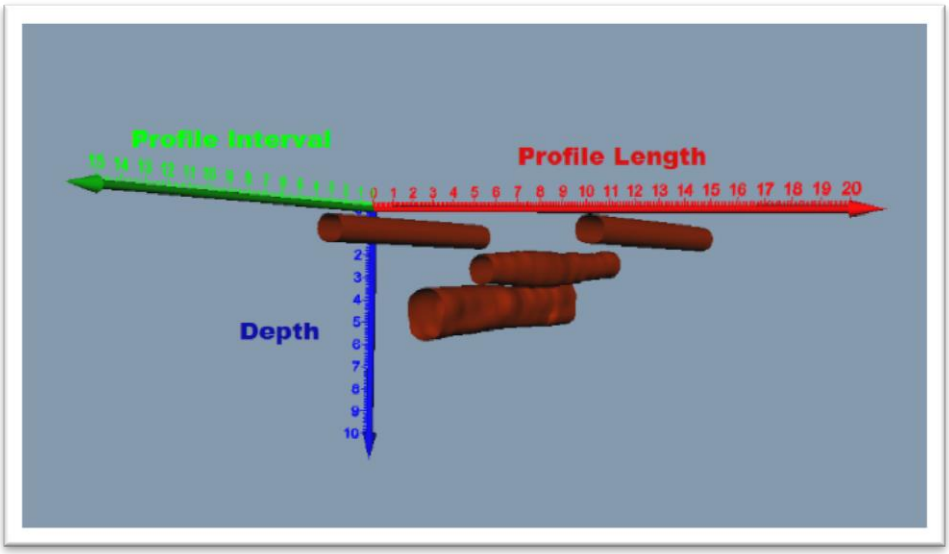

Fig.15. Isosurface generated with Voxler 4.0 (units are in meters)

They were produced in a way that the anomalies of existing utilities can be distinguished in the 3D modeling process carried out with the radargrams obtained from the simulation data. Figures 14, 15, and Figure S2(in Supplementary) show the direction of lines and the difference in slope applied to 2 pipelines. The 3D modeling based on Voxler 4.0 software allows for removing unnecessary parts from the gained surface and bringing the desired attributes to the forefront.

Experiments

The measurements were performed on the rainwater drainage pipeline with a length of about 15 meters, a diameter of 30 cm, and a depth of 40 cm, which is located at the junction of two grates in the parking lot of the Davutpasa Campus of the Faculty of Civil Engineering, Yıldız Technical University.

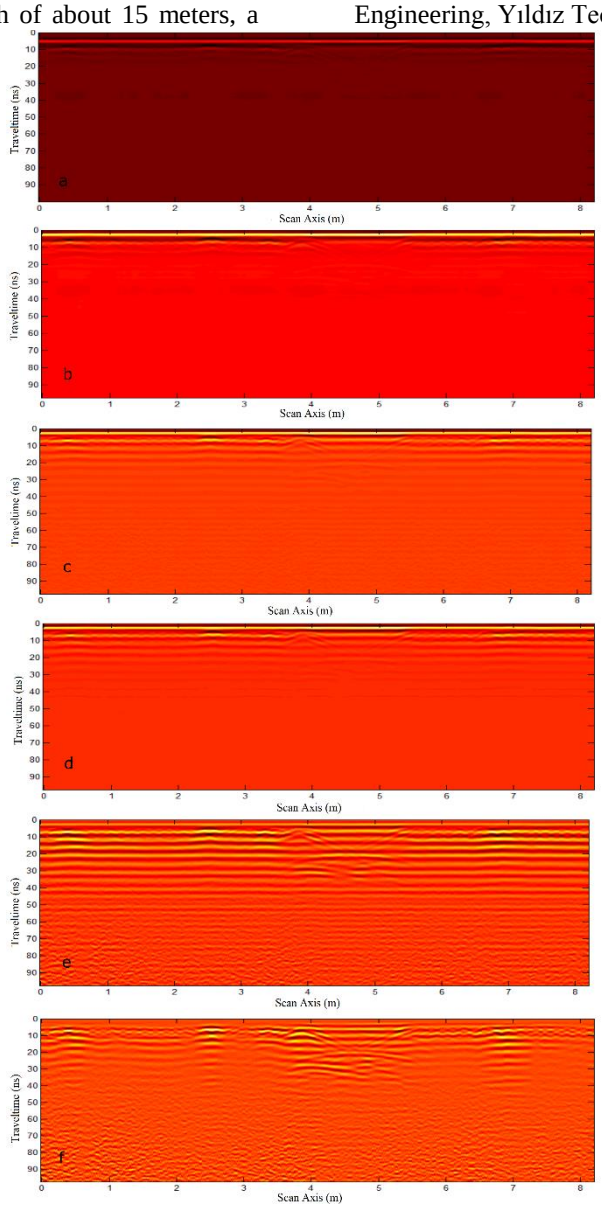

Fig. 16. a. Raw data b. Signal Adjusting c. Dewow d. Bandpass Filtering e. Gain f. Backgroung Removal

The radargrams of the measurement performed with Geoscanner GCB GPR with a center frequency of 300 MHz were analyzed with MatGPR 3.1 software. The process steps in Figure 6 were applied to each radargram. Figure 16 demonstrates the example radargram obtained from the field and the applied process steps.

The velocity and depth were calculated using Equation (1) and Equation (2). The velocity was found 0.12 m/ns, the depth 1.16 m and the radius 0.1412 m (Figure 17). However, it is seen that the depth calculated based on the actual information does not coincide with the depth of utility under measurement. It was seen that when the migration process was performed based on the obtained velocity, the reflection gave a linear result other than a point result (Figure 18b).

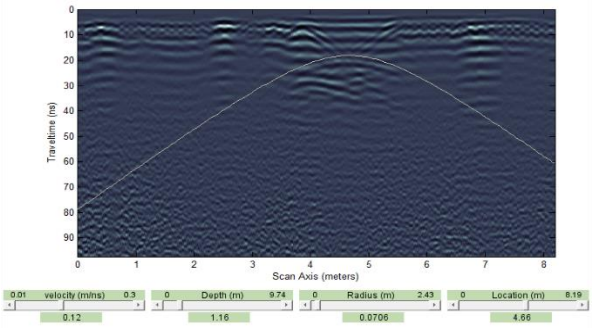

Fig. 17. Determination of velocity, depth, radius and location from hyperbola reflection on radargram.

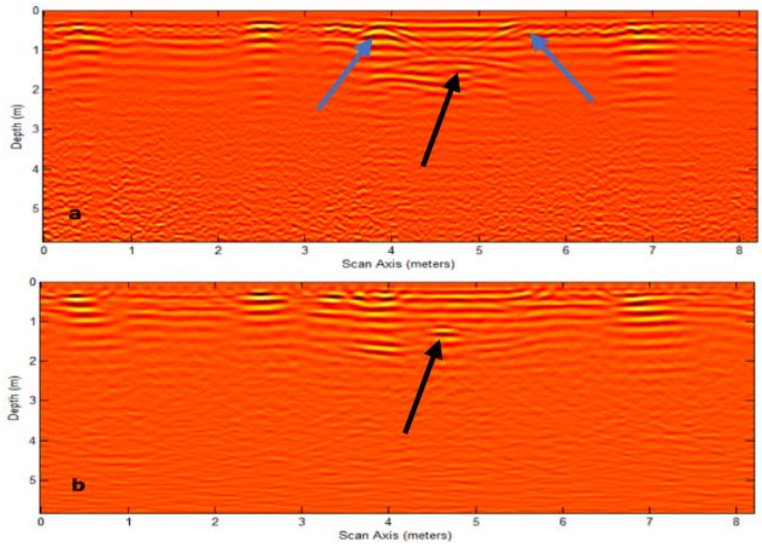

Fig. 18: a. Time-depth Conversion b. Migration

If the hyperbola reflection was caused by the pipe, the migration process would have given a point result at the peak of the hyperbola. When the consecutive radargrams were investigated, it was seen that the hyperbola reflections were different and lost in some of them (Figure S1 in Supplementary). If it was a utility reflection, it would have also been seen as hyperbola in others. This suggested that the reflection is a pseudo-reflection.In the literature, it is stated that such reflection may occur when the trench base is narrow (Goodman and Piro, 2013).

When the field study results were evaluated, it was seen that there was no reflection for the pipeline. However, the study contains results suggesting that utility work has been performed. When a portion of the processed radargrams on the horizontal axis of 4-5 meters and the vertical axis of 0-0.5 m was examined, the start and end points of the trench (trench width) shown by blue arrow in Figure 18a can be seen.

Considering the pipe diameter to be detected, it is seen that the wavelength corresponding to the antenna frequency used is sufficient to detect the pipeline. When Table 2 is examined, the center frequency wavelength will be between 0.26-0.45 meters. This wavelength range appears to be suitable for a pipe with a diameter of 30 cm.

Table 2.The wavelength corresponding to the center frequency and dielectric coefficient. (Conyers and Goodman, 1997).

Antenna Frequency (MHz)	**ε_r=1**	**ε_r=5**	**ε_r=15**	**ε_r=25**	
1000	0.30	0.13	0.08	0.06	
900	0.33	0.17	0.09	0.07	
500	0.60	0.27	0.15	0.12	
300	1	0.45	0.26	0.20	
120	2.50	1.12	0.65	0.50	**Wavelength (m)**
100	3	1.34	0.77	0.60	
80	3.75	1.68	0.97	0.75	
40	7.5	3.35	1.94	1.50	
32	9.38	4.19	2.42	1.88	
20	15	6.71	3.87	3	
10	30	13.42	7.75	6	

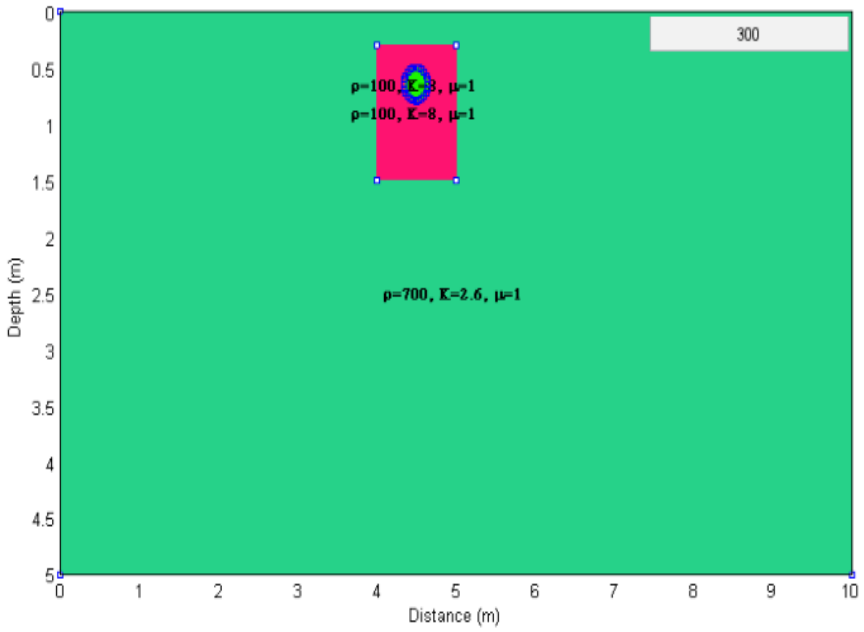

Fig.19. The simulation model containing objects with the same dielectric constant.

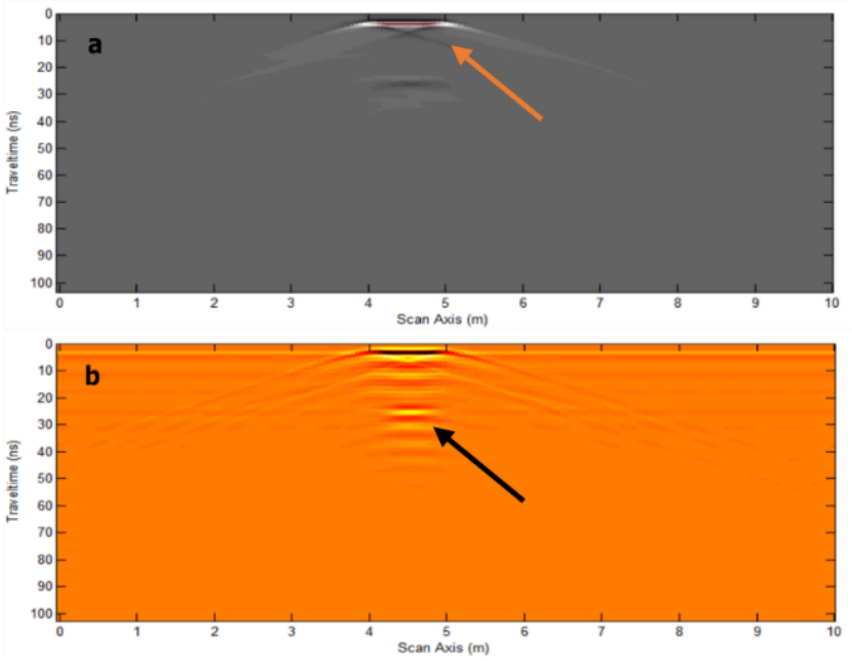

Fig. 20. a. Raw radargram b. Processed radargram.

So the hyperbola reflection of the utility could not be obtained in the field study was considered a situation that may be encountered if the medium and the utility have similar characteristics. To examine this possibility, a simulation model was established so that the pipeline remained within another object with the same dielectric constant as itself. The established model is shown in Figure 19. As is seen in the raw and processed radargrams (Figure 20a and Figure 20b), no hyperbola reflection was obtained from the pipe with the same dielectric constant as the object surrounding it. Only the reflections relating to the upper (shown by arrow in Figure 20a) and lower (shown by arrow in Figure 20b) part of the object surround the pipe are seen. It is thought that the situation encountered in the field study was due to this. Since the reflection relating to the utility could not be obtained in the field study, 3-D Modeling could not be made for the utility.

Conclusion

Considering the study performed based on the simulation model, the determination of information on utilities with different dielectric constants using a GPR seems possible. When the results obtained based on the simulation model were investigated, the location and depth differences were found at 1 cm, and the diameter differences were found at 1.42 cm and 1.5 cm, respectively, in the utilities (P.W1 and P.W2) close to the surface. For the utilities located at a deeper level, the location difference was found 1 cm, the depth difference was found 1-5 cm for S.W and 15-18 cm for

W.W, and the diameter difference was found 6.6 cm for S.W and 12.8 cm for W.W. Also, the slope of -2% given for both lines was found -2.1% for S.W and -2.2% for W.W at the end of the evaluation. As is seen, the deviation is smaller in the lines close to the surface, while it increases in the lines located at a deeper level. This may be caused by the attenuation of the electromagnetic wave in time.

When we evaluate the results in terms of the field study, two basic results stand out. One of them is the consideration of the fact that every hyperbola does not come from a pipeline. A rock with an oval surface or narrow trench bases may give such hyperbola reflections. The hyperbola reflection seen in the field study is an indication of this situation. It can be solved by the interpretation of consecutive radargrams.

The other result is the fact that the dielectric constants of utility and its surrounding are important. Because one of two objects with the same dielectric constant may prevent the other from being obtained. Although no reflection relating to a pipeline was seen in the field study, the excavation traces seen on the radargrams, in other words, reflections from ground changes, may allow for making interpretations about the trench width and depth.

The conspicuous limitation of the study is that test excavation may be needed as there may be misinterpretations, and if GPS support is not available, the borders of the profiles are marked on the ground and measured before excavation to locate the underground changes accurately.

References

Anspach, J.H., (1996). "Subsurface Utility Engineering: Utility Detection Methods and Applications", *Society of Exploration Geophysicists*, 443-449, doi.10.4133/1.2922301

Blindow, N., Eisenburger, D., Illich, B., Petzold, H., and Richter, T. (2007). Ground penetrating radar. In Environmental Geology (pp. 283-335). Springer, Berlin, Heidelberg.

Costello, S., Chapman, D., Rogers, C. & Metje, N., (2007). "Underground Asset Location and Condition Assessment Technologies", *Tunnelling and Underground Space Technology*, 22: 524-542, doi.10.1016/j.tust.2007.06.001

Daniels, J.J., (1989). "Fundamentals of ground penetrating radar": *Society of Exploration Geophysicists*, 62-142.

Chow, T. and Rees, H., (1989). "Identification of subsurface drain locations with ground-penetrating radar", *Canadian Journal of Soil Science*, 69: 223-234, doi.10.4141/cjss89-023

Conyers, L. B., Goodman, D. (1997). *Ground-penetrating radar: an introduction for archaeologists. AltaMira press.*

Goodman, D. Piro, S., (2013). GPR remote sensing in archaeology: Springer.

Golden Software, (2015). Voxler4 Ouick Start Guide, Colorado, USA.

GPR, (2017). https://lostclipper.files.wordpress.com/

Kurt, B.B., Kadıoğlu, S. Ekincioğlu, E.E., (2009). "Yer radarı yöntemi ile gömülü boruların konum, büyüklük ve fiziksel özellikleri ile belirlenmesi", *Yerbilimleri/Hacettepe Üniversitesi Yerbilimleri Uygulama ve Araştırma Merkezi Dergisi,* 30: 45-57.

Leckebusch, J., (2003). "Ground- penetrating radar: a modern three- dimensional prospection method", Archaeological Prospection, 10: 213-240, doi.10.1002/arp.211

Jeng, Y. and Chen, C. S. (2012). Subsurface GPR imaging of a potential collapse area in urban environments. Engineering Geology, 147, 57-67, doi.10.1016/j.enggeo.2012.07.009

Jol, H.M., (2008). Ground penetrating radar theory and applications, Elsevier, U.K.

Metwaly, M., (2015). "Application of GPR technique for subsurface utility mapping: A case study from urban area of Holy Mecca, Saudi Arabia", Measurement, 60: 139-145, doi.10.1016/ j.measurement.2014.09.064

Öztürk, C., (2011). Yeraltına Nüfuz Eden Radar (Yner) Modellemesinde Işın İzleme Ve Fdtd Yöntemlerinin Karşılaştırılması, Doktora Tezi. Dokuz Eylül Üniversitesi.

Prego, F. J., Solla, M., Puente, I., Arias, P., 2017. Efficient GPR data acquisition to detect underground pipes. *NDT and E International*, 91, 22-31, doi.10.1016/j.ndteint.2017.06.002

Ristic, A. V., Petrovacki, D., and Govedarica, M., 2009. A new method to simultaneously estimate the radius of a cylindrical object and the wave propagation velocity from GPR data. *Computers and Geosciences*, 35(8), 1620-1630, doi.10.1016/j.cageo.2009.01.003

Šarlah, N., Podobnikar, T., Ambrožič, T., & Mušič, B. (2020). Application of Kinematic GPR-TPS Model with High 3D Georeference Accuracy for Underground Utility Infrastructure Mapping: A Case Study from Urban Sites in Celje, Slovenia. *Remote Sensing*, 12(8), 1228.

This, A., 2010. Mate PR Release 2: A freeware MATLAB® package for the analysis and interpretation of common and single offset GPR data. FastTimes, 15 (1), 17 – 43.

URL1. Uçar S. Türkiye'de Kazı Kaynaklı Doğal Gaz Boru Hattı Hasarları, Etkin Müdahale Usulleri, Kazı Hasarlarının Önemli Ölçüde Azaltılamsı İçin Öneriler ve İnovatif Sistem Örneği (In Turkish). http://www.gazmer.com.tr/dokumanlar/156688910 7-d.pdf. Last Accessed Date: 05 October 2021.

URL2.Sensors&Software, www.sensoft.ca/blog/what-is-gpr/.

Supplementary

Table S1. Pipe Comparison. D: Diameter, De: Depth, E: Estimated, Loc: Location, R: Radargram

Pipe Type	Radargram	Loc. (m)	De (m)	D (m)	E.Loc (m)	E.De (m)	E.D (m)	Δl (m)	Δz (m)	Δr (m)
P.W 1	R.*	5.20	1.00	0.18	5.21	1.01	0.166	-0.01	-0.01	0.0142
P.W 2	R.*	14.60	1.00	0.16	14.61	1.01	0.145	-0.01	-0.01	0.015
S.W	R1	11.00	2.00	0.30	11.01	2.03	0.234	-0.01	-0.03	0.066
	R6	11.00	2.02	0.30	11.01	2.03	0.234	-0.01	-0.01	0.066
	R11	11.00	2.04	0.30	11.01	2.05	0.234	-0.01	-0.01	0.066
	R16	11.00	2.06	0.30	11.01	2.08	0.234	-0.01	-0.02	0.066
	R21	11.00	2.08	0.30	11.01	2.11	0.234	-0.01	-0.03	0.066
	R26	11.00	2.10	0.30	11.01	2.11	0.234	-0.01	-0.01	0.066
	R31	11.00	2.12	0.30	11.01	2.14	0.234	-0.01	-0.02	0.066
	R36	11.00	2.14	0.30	11.01	2.17	0.234	-0.01	-0.03	0.066
	R41	11.00	2.16	0.30	11.01	2.19	0.234	-0.01	-0.03	0.066
	R46	11.00	2.18	0.30	11.01	2.22	0.234	-0.01	-0.04	0.066
	R51	11.00	2.20	0.30	11.01	2.25	0.234	-0.01	-0.05	0.066
W.W	R1	9.00	3.20	0.50	9.01	3.37	0.372	-0.01	-0.17	0.128
	R6	9.00	3.22	0.50	9.01	3.38	0.366	-0.01	-0.16	0.134
	R11	9.00	3.24	0.50	9.01	3.41	0.372	-0.01	-0.17	0.128
	R16	9.00	3.26	0.50	9.01	3.41	0.372	-0.01	-0.15	0.128
	R21	9.00	3.28	0.50	9.01	3.45	0.372	-0.01	-0.17	0.128
	R26	9.00	3.30	0.50	9.01	3.45	0.372	-0.01	-0.15	0.128
	R31	9.00	3.32	0.50	9.01	3.47	0.372	-0.01	-0.15	0.128
	R36	9.00	3.34	0.50	9.01	3.5	0.372	-0.01	-0.16	0.128
	R41	9.00	3.36	0.50	9.01	3.53	0.372	-0.01	-0.17	0.128
	R46	9.00	3.38	0.50	9.01	3.55	0.372	-0.01	-0.17	0.128
	R51	9.00	3.40	0.50	9.01	3.58	0.372	-0.01	-0.18	0.128

*All values valid from R1 to R51.

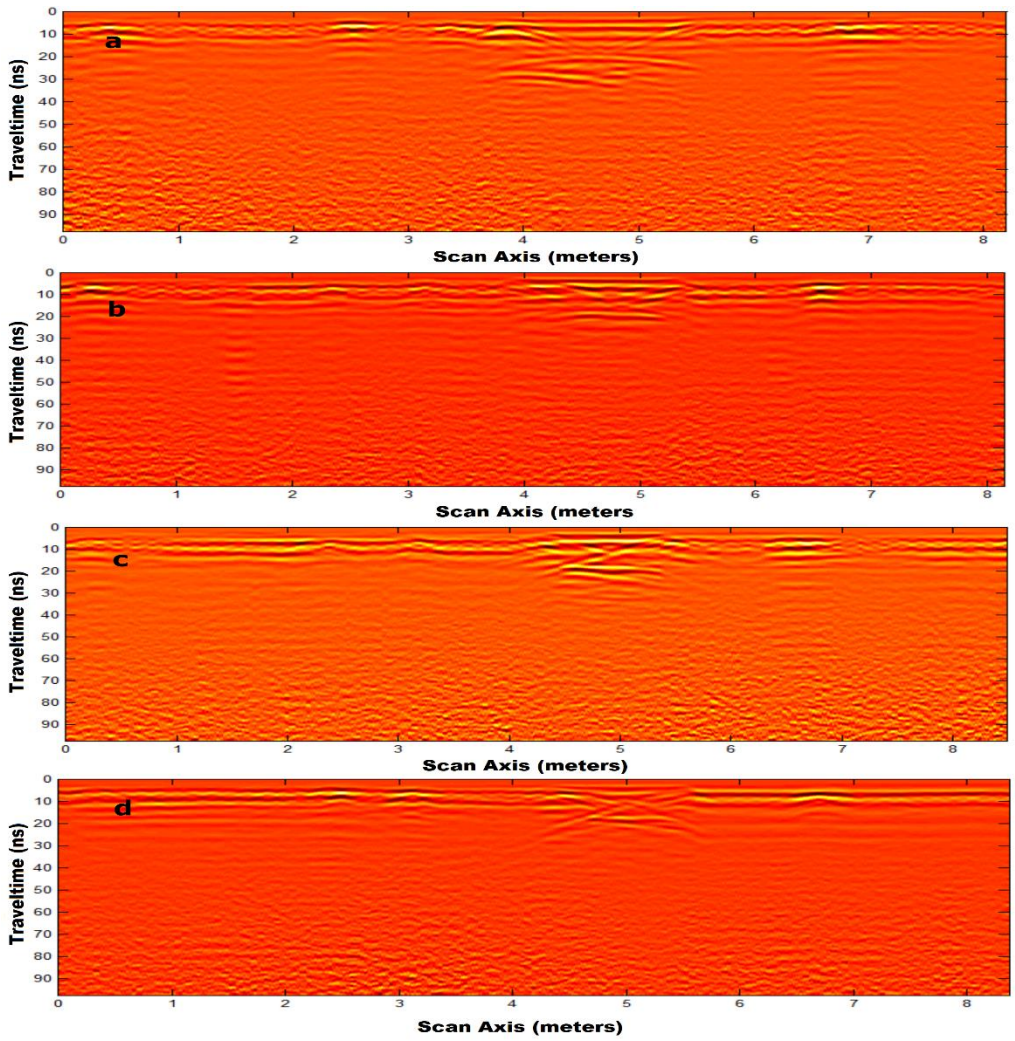

Fig. S1: A.Radargram 3 b. Radargram 4 c. Radargram 5 d. Radargram 6.

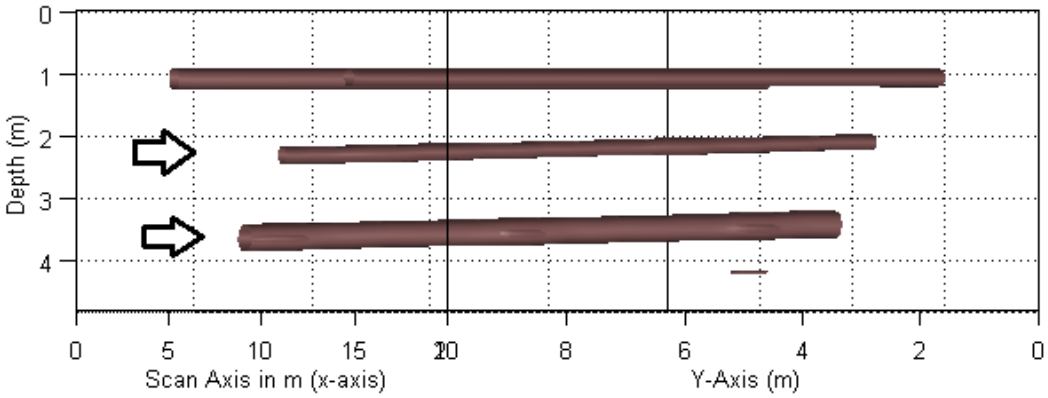

Fig. S2: The Slope Difference.